Ab initio calculations of residual resistivities for dilute Ni alloys

I. Mertig
Technische Universität Dresden, Sektion Physik, Institut für Theoretische Physik, 8027 Dresden, Germany

R. Zeller and P. H. Dederichs
Institut für Festkörperforschung, Forschungszentrum Jülich, D-5170 Jülich, Germany
(Received 3 September 1992; revised manuscript received 10 March 1993)

We report residual resistivity calculations for dilute Ni alloys which are based on density-functional theory and the Korringa-Kohn-Rostoker Green's-function method. The transport is described quasiclassically by means of the Boltzmann equation using a two-current model for the ferromagnetic host. In particular we consider 3*d*, 4*d*, 4*sp*, and 5*sp* impurities in Ni and include in addition to the impurity potential one shell of perturbed host potentials in the calculation. For the residual resistivity, satisfactory agreement with the experiments is obtained in practically all cases. We clarify the role of both subbands for the transport properties and compare the calculated ratios of subband resistivities with experimentally determined values.

I. INTRODUCTION

Following Mott's idea,[1] several transport properties of ferromagnetic alloys can be explained by assuming conduction in parallel by electrons in the majority bands (spin-up electrons) and by electrons in the minority bands (spin-down electrons) . The physical basis of this two-current model is the dominance of spin-conserving potential scattering and the weakness of spin-flip collisions in a ferromagnetic alloy at low temperatures. This model has been used by many authors[2–9] for studies on Ni-based alloys. It seems that the model provides a good basis for the discussion of a wide range of alloy properties.[10] Owing to the developments of density-functional theory and sophisticated numerical techniques we are now able to perform realistic *ab initio* calculations and we are in a position to check the reliability of such model studies mentioned above. Recent theoretical studies of dilute Ni alloys by Blügel and co-workers,[11] by Stefanou and co-workers,[12] and by Zeller[13] presented a detailed analysis of the range of charge and magnetization perturbations around impurities in Ni, performed within the Korringa-Kohn-Rostoker (KKR) Green's-function method. This work is an extension of the same formalism to transport properties of dilute Ni alloys. For this purpose the microscopic transition probability for an impurity atom with perturbed neighboring potentials around the impurity is calculated and feeded into the Boltzmann equations for the spin-up and spin-down electrons. The transport equation was then solved by iteration as proposed by Coleridge[14] and van Ek and Lodder[15] for nonmagnetic materials. Within this scheme a detailed analysis of the spin-up and spin-down contributions to the residual resistivity becomes feasible without introducing any free parameters.

The outline of the paper is as follows. In Sec. II the microscopic scattering probability is derived within the Green's-function method. Sec. III gives a description of the solution of the transport equation. In Sec. IV methodical aspects are presented and in Sec. V the results are discussed.

II. MICROSCOPIC TRANSITION PROBABILITY

The transition from a state k into a state k', where k is a shorthand notation for the wave vector $\mathbf{k}$ and the band index ν, is given by

$$P_{kk'} = 2\pi c|T_{kk'}|^2\delta(\varepsilon_k - \varepsilon_{k'})\,, \tag{1}$$

where c is the atomic concentration of impurities. Within the powerful KKR Green's-function formalism[16–19] the transition matrix elements $T_{kk'}$ for the scattering of Bloch electrons by an impurity cluster embedded in an ideal host crystal are given by

$$T_{kk'} = \frac{\hbar^2}{2m}\frac{1}{\sqrt{E_F}}\sum_{Ln} C_L^n(k)Q_L^n(k'). \tag{2}$$

L denotes a pair of angular momentum indices, i.e., $L = (l, m)$ and n characterizes the sites of the perturbed potentials in the cluster. $C_L^n(k)$ and $Q_L^n(k)$ are generalized wave-function coefficients for the host and the alloy, respectively. The latter are connected by the relation

$$Q_L^n(k) = \sum_{L'n'} T_{LL'}^{nn'} C_{L'}^{n'}(k). \tag{3}$$

Neglecting lattice distortion effects the T-matrix coefficients $T_{LL'}^{nn'}$ contain the structural Green's-function matrix elements $G_{LL'}^{nn'}$ (Refs. 17–19) of the perturbed system

$$T_{LL'}^{nn'} = e^{-i\eta_l^0}\Delta t_l^n(1 + G_{LL'}^{nn'}\Delta t_{l'}^{n'})e^{-i\eta_{l'}^0}\,. \tag{4}$$

Here η_l^0 are the scattering phase shifts of the unperturbed potentials, and Δt_l^n represents the differences between

the single-site t matrices of the perturbed potentials and the unperturbed ones. The structural Green's-function matrix $G^{nn'}_{LL'}$ contains all the information about multiple scattering between the perturbed muffin tins and can be related to its counterpart for the host crystal by an algebraic Dyson equation.[12,13] Substitution of Eqs. (2), (3), and (4) in Eq. (1) results in

$$P_{kk'} = c\left(\frac{\hbar^2}{2m}\right)^2 \frac{1}{E_F}\,\delta(\varepsilon_k - \varepsilon_{k'}) \times \sum_{LL'nn'} Q^{n*}_L(k) Q^{n'}_{L'}(k) C^n_L(k') C^{n'*}_{L'}(k'). \quad (5)$$

III. TWO-CURRENT MODEL

Two-current (or two-band) models have often been used to describe the electrical conduction in metals. One assumes that two groups of electrons carry current independently and in parallel to each other.[1]

In ferromagnetic alloys we consider two subgroups of charge carriers, i.e., the spin-up and the spin-down electrons, characterized by the quantum numbers $k = (\mathbf{k}, \nu)$ and spin index σ. Both spin directions contribute separately to the resistivity. In the dilute limit $c << 1$ the residual resistivity of impurities can be obtained from the solution of the linearized Boltzmann equation

$$\mathbf{\Lambda}^\sigma_k = \tau^\sigma_k \left(\mathbf{v}^\sigma_k + \sum_{\sigma'}\sum_{k'} P^{\sigma\sigma'}_{kk'} \mathbf{\Lambda}^{\sigma'}_{k'}\right) \quad (6)$$

for the vector mean free path $\mathbf{\Lambda}^\sigma_k$. Here $\mathbf{v}^\sigma_k$ is the Fermi velocity and τ^σ_k is the electron lifetime due to impurity scattering

$$\tau^{\sigma\,-1}_k = \sum_{\sigma'}\sum_{k'} P^{\sigma\sigma'}_{kk'} = -2c\,\mathrm{Im}T^{\sigma\sigma}_{kk}. \quad (7)$$

The second equality in (7) expresses the optical theorem connecting diagonal elements of the transition matrix $T_{kk'}$ [Eq. (2)] to a sum over all transition probability rates for scattering out of state (k, σ).

Obviously, Eq. (5) represents a system of coupled integral equations for the vector mean free path $\mathbf{\Lambda}^\sigma_k$ of all states (k, σ).

Finally, we obtain two currents with the density

$$\mathbf{j}^\sigma = e^2 \sum_k \delta(\varepsilon_k - \varepsilon_F)\, \mathbf{v}^\sigma_k\, (\mathbf{\Lambda}^\sigma_k\, \mathbf{E}). \quad (8)$$

Comparing with $\mathbf{j}^\sigma = (\hat{\rho}^\sigma)^{-1}\mathbf{E}$, two resistivity contributions

$$(\rho^\sigma)^{-1}_{ij} = e^2 \sum_k \delta(\varepsilon_k - \varepsilon_F)\, v^\sigma_{k\,i}\, \Lambda^\sigma_{k\,j}$$

are derived, $\hat{\rho}^\uparrow$ for the majority electrons and $\hat{\rho}^\downarrow$ for the minority ones.

Due to the parallel addition of the two currents the total resistivity for cubic systems becomes

$$\rho = \frac{\rho^\uparrow + \rho^\downarrow}{\rho^\uparrow \rho^\downarrow} \qquad \text{using} \qquad \hat{\rho}^\sigma_{ij} = \rho^\sigma \delta_{ij}. \quad (9)$$

With respect to the dependence on the spin-quantum number the scattering probability in Eq. (6) consists of four parts

$$P^{\sigma\sigma'}_{kk'} = \begin{pmatrix} P^{\uparrow\uparrow}_{kk'} & P^{\uparrow\downarrow}_{kk'} \\ P^{\downarrow\uparrow}_{kk'} & P^{\downarrow\downarrow}_{kk'} \end{pmatrix}, \quad (10)$$

two spin-conserving scattering processes $P^{\uparrow\uparrow}_{kk'}$ and $P^{\downarrow\downarrow}_{kk'}$ and two spin-flip contributions $P^{\uparrow\downarrow}_{kk'}$ and $P^{\downarrow\uparrow}_{kk'}$. From this point of view the spin-flip processes lead to a momentum transfer between the currents.

There are several mechanisms of spin mixing such as scattering with spin waves[20] and collisions between spin-up and spin-down electrons,[21] both of which vanish at zero temperature. But there are also residual spin-mixing terms. Firstly, there is a spin-flip scattering by the impurities due to spin-orbit coupling which has an about 100 times smaller cross section than spin-conserving potential scattering.[22] Finally, spin mixing at $T = 0$ can result from the combined action of the internal magnetic induction and the spin-orbit coupling. Since in the presence of spin-orbit coupling the spin is no longer a good quantum number the probability for a Bloch electron k to be in a spin-up or spin-down state coherently oscillates between both directions. The resulting spin-flip term is independent of the impurities and so is very important in alloys with small residual resistivities below about 1 $\mu\Omega$ cm at. %.[23]

In this paper we assume that for the Ni alloys this residual spin mixing can be neglected. We will discuss in Sec. V the consequences and limits of this approximation. Without spin mixing Eq. (6) decouples for both spin directions, and with the spin-conserving transition probability $P^{\sigma\sigma}_{kk'}$ of Eq. (10) the Boltzmann equations can be rewritten as

$$\mathbf{\Lambda}^\sigma_k = \tau^\sigma_k \left[\mathbf{v}^\sigma_k + P_0 \sum_{LL'nn'} Q^{n\sigma}_L(k) Q^{n'\sigma\,*}_{L'}(k) \Xi^{nn'\sigma}_{LL'}\right] \quad (11)$$

with Fermi surface integrals

$$\Xi^{nn'\sigma}_{LL'} = \sum_{k'} \delta(\varepsilon_k - \varepsilon_{k'}) C^{n\sigma}_L(k') C^{n'\sigma}_{L'}(k') \mathbf{\Lambda}^\sigma_{k'}. \quad (12)$$

Generally, the integrals (12) can be solved exactly because of the degenerate integral kernel.[24] Instead of the integral equation an algebraic set of rank $R = (L \times L' \times n \times n')^2$ would have to be solved, which is, for example, for angular momenta up to $l = 3$ and 13 perturbed atoms in the cluster: $R = (16 \times 16 \times 13 \times 13)^2 \cong 2 \times 10^9$, clearly too large for a numerical treatment.

Consequently, we solved Eq. (11) by iteration as it was proposed by Coleridge[14] and van Ek and Lodder[15] for nonmagnetic systems. As a starting value we tried several expressions such as the relaxation-time approximation

$$\mathbf{\Lambda}^{\sigma\,0}_k = \tau^\sigma_k \mathbf{v}^\sigma_k \quad (13)$$

or the Ziman approximation

$$\Lambda_k^{\sigma Z_i} = \mathbf{v}_k^\sigma \frac{1}{\sum_{k'} \delta(\varepsilon_k - \varepsilon_{k'})(1 - \mathbf{v}_k^\sigma \mathbf{v}_{k'}^\sigma) P_{kk'}^{\sigma\sigma}} \tag{14}$$

or the degenerate kernel solution for the single-site case. In all cases convergence was achieved without significantly different convergence rates. The mean free paths utilized were assumed to be converged if for all points on the Fermi surface the largest relative change in $\mathbf{\Lambda}_k^\sigma$ between two subsequent iterations, i and $i+1$, was less than 10^{-5},

$$\max\left[\frac{\|\mathbf{\Lambda}_k^\sigma(i+1) - \mathbf{\Lambda}_k^\sigma(i)\|}{\|\mathbf{\Lambda}_k^\sigma(i)\|}\right] < 10^{-5}.$$

This criterion was met for all systems with $\rho \geq 1\ \mu\Omega\,\mathrm{cm/at.\,\%}$ within 10 iterations.

IV. METHOD

This section specifies the numerical details in the calculation. A basic ingredient is the self-consistent potential for pure Ni which is taken from Moruzzi, Janak, and Williams.[25] The KKR method with an angular momentum truncation at $l_{\max} = 4$ was used.

The imaginary part of the structural Green's function was generated within the same KKR method by means of a Brillouin-zone integration using the tetrahedron method.[26,13] The real part of the Green's function was calculated by a Hilbert transformation[13] with a truncation energy of 2.0 Ry.

The self-consistent impurity calculations are performed within the frame of density-functional theory[27,28] using the local spin-density approximation as proposed by von Barth and Hedin[29] with parameters as chosen by Moruzzi, Janak, and Williams.[25] To obtain the Green's function of the perturbed system the algebraic Dyson equation is solved. The dimension of this equation is made finite by truncating the angular momentum expansion at $l = 3$ and by assuming potential perturbations only at the impurity site and at the first-shell atoms around the impurity.

The necessary Fermi surface integrations were performed with a modified tetrahedron method.[19]

V. RESULTS AND DISCUSSION

The Fermi surface of Ni consist of five sheets[40] of the electronlike majority Fermi surface $e_6^\uparrow$ [Fig. 1(a)] and four sheets of the minority Fermi surface, two holelike ones $h_3^\downarrow, h_4^\downarrow$ [Figs. 1(b)and 1(c)], and two electronlike ones $e_5^\downarrow, e_6^\downarrow$ [Figs. 1(d)and 1(e)].

The band projection of the partial densities of states at the Fermi energy (see Table I) are a measure for the character of the electronic states. From Table I it becomes obvious that the majority band includes a mixture of a smaller contribution of sp states and a larger one of d states whereas the minority bands are strongly dominated by the d states.

The results for the residual resistivities of $3d$ and $4sp$ impurities are shown in comparison with the experimental results in Fig. 2(a). The subband resistivities $\rho^\uparrow$ and $\rho^\downarrow$ are presented in Fig. 2(b), while Fig. 2(c) gives the relative contributions of different Fermi surface sheets to the conductivity.

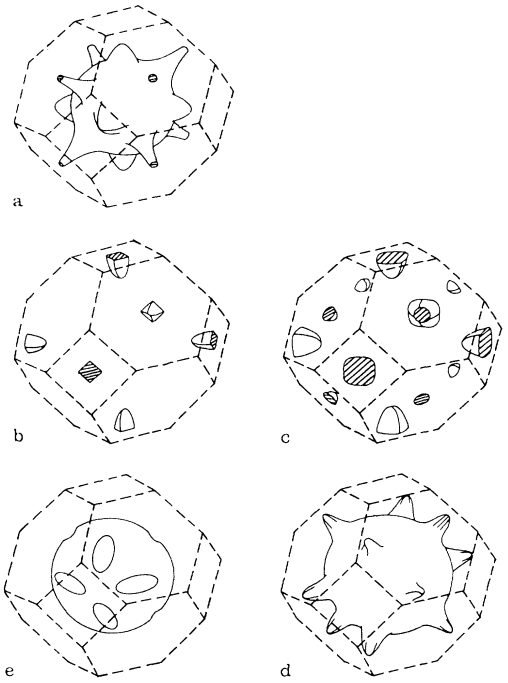

FIG. 1. Ni Fermi surface (Ref. 40). Majority sheet: (a) $e_6^\uparrow$. Minority sheets: (b) $h_3^\downarrow$, (c) $h_4^\downarrow$, (d) $e_5^\downarrow$, (e) $e_6^\downarrow$.

The corresponding data for impurities of the $4d$ and $5sp$ series are given in Fig. 3.

The data are also listed in Tables II, III, and IV. Contrary to the more accurate values $\rho^\sigma_{\text{1 shell}}$, which include the perturbed potentials of the nearest-neighbor host atoms, the resistivities $\rho^\sigma_{\text{single site}}$ include the effect of the impurity potential alone.

A. 3d impurities

According to the calculation of Zeller,[13] the local density of states (LDOS) of the majority electrons is practically unchanged for Co and Fe impurities. This is especially true for the LDOS at E_F. Since also the neighboring potentials are unchanged,[12,13] the spin-up resistivity $\rho^\uparrow$ is extremely small. For Mn impurities a sharp virtual bound state (VBS) separates from the majority d band. However, only a small tail of this state becomes unoccupied so that the resistivity $\rho^\uparrow$ increases moderately. For Cr impurities the majority VBS is located slightly above E_F, leading to a strong resonance scattering for the majority electrons. In the sequence V, Ti, Sc the majority VBS moves to higher energies, so that the majority resistivity $\rho^\uparrow$ decreases. From Table II it can be seen that for the majority band the single-site approximation gives reliable resistivities. This is a consequence of the fact that the spin perturbations $\delta N^\uparrow$ of the neighboring host atoms are rather small (see Table II of Ref. 12). In cor-

TABLE I. Fermi surface characteristics. The angular brackets denote a Fermi surface average $\langle\,\rangle = \sum_k \delta(\varepsilon_k - \varepsilon_F)\cdots$. $N_l(E_F)$ is the band projected partial density of states at the Fermi energy. All parameters are given in a.u. In the last column the number of k points at the Fermi surface in the irreducible part of the Brillouin zone is given. These k points contribute to the necessary Fermi surface integrations.

	Fig. 1	Area	$\langle v_k^2 \rangle$	$N_s(E_F)$	$N_p(E_F)$	$N_d(E_F)$	k points
$e_6^\uparrow$	(a)	7.9	5.6	1.237×10^{-2}	2.559×10^{-2}	1.176×10^{-1}	460
$h_3^\downarrow$	(b)	2.0	0.5	1.006×10^{-4}	1.573×10^{-3}	4.124×10^{-2}	43
$h_4^\downarrow$	(c)	22.9	4.4	1.443×10^{-4}	2.362×10^{-4}	9.789×10^{-2}	69
$e_5^\downarrow$	(d)	25.7	9.9	1.221×10^{-3}	6.706×10^{-3}	1.146×10^{0}	809
$e_6^\downarrow$	(e)	11.4	4.3	4.769×10^{-3}	7.171×10^{-3}	2.109×10^{-1}	360

respondence to the character of states as well as d-d, s-s, and s-d scattering occurs and influences the resistivity.

Compared to the majority band, the scattering in the minority band is generally much stronger, so that with exception of Cr, V, and Ti one has for the subband resistivities $\rho^\downarrow > \rho^\uparrow$. This is in line with the strong changes of the minority population upon alloying, as, e.g., discussed in Ref. 12. Already for Co impurities the minority VBS is above E_F and moves further away for Fe and Mn. Due to the missing states at the upper edge of the Ni minority band, i.e., at E_F, we have a strong scattering at the "hole states" of the missing Ni atom, which is about the same for all $3d$ impurities from Fe to Sc. The small dip of $\rho^\downarrow$ at Cr is connected with the flip of the local moment, which brings the minority VBS back to the Fermi energy. From Table II it can be seen that an important contribution to $\rho^\downarrow$ comes from the perturbed neighboring host potentials being in line with the large changes for $\delta N^\downarrow$ for the nearest neighbors as found in Ref. 12. Inside the minority band the main contribution stems from $e_5^\downarrow$ [see Fig. 2(c)].

Due to the parallel addition of the two subband currents, the total resistivity ρ is dominated by the majority resistivity $\rho^\uparrow$, as is clearly demonstrated in Figs. 2(a) and 2(b). All trends of ρ are determined by $\rho^\uparrow$, since for all $3d$ impurities except Cr, V, and Ti $\rho^\uparrow < \rho^\downarrow$. Therefore also the perturbations of the neighboring atoms, while strongly affecting $\rho^\downarrow$, are of minor importance for the total resistivity. The calculated ρ values agree reasonably well with the experimental data, except that there seems to be a systematic underestimation of the resistivity for Fe, Co, Cu, and Zn impurities. At least partially this is due to the neglect of spin-flip scattering. Here the finite experimental values are strongly influenced by the spin-orbit interaction being neglected in the calculation. Via spin-orbit coupling in the host band the strong scattering in the minority bands also leads to an appreciable scattering in the majority bands which then determines the total resistivity. A fully relativistic *ab initio* treatment would therefore be very desirable.

B. 4*d* impurities

From the electronic-structure point of view, $4d$ impurities differ from the $3d$ counterparts due to the stronger hybridization with the Ni d band and due to the weaker tendency for magnetism, i.e., the smaller exchange integrals. The electronic structure of these impurities in Ni has been calculated by Zeller[13] and the present results can essentially be understood from the LDOS presented there. The characteristic feature of the LDOS for the $4d$ impurities is a two-peak structure for both bands, with one peak at the lower edge of the $3d$ band and one at the upper end. This splitting is directly caused by the strong $4d$-$3d$ hybridization being much larger than the $3d$-$3d$ hybridization in pure Ni.

For Pd the LDOS at E_F is only weakly distorted and one obtains a very small resistivity in both bands. In the sequence Rh, Ru, to Tc the upper d peak of the majority band moves to the Fermi energy which explains the strong resonance scattering of the majority electrons for Tc impurities for which the peak is directly at E_F. By further proceeding to Mo, Nb, Zr, and Y impurities the peak shifts above E_F and the majority resistivity decreases again. As in the $3d$ series, the resistivity in the minority band is essentially determined by the missing d states at E_F and the resistivity is more or less constant from Y to Tc. As a consequence of the strong $4d$-$3d$ hybridization the contributions to the resistivity from the neighboring potentials is more important than in the $3d$ series and the resistivities are in general somewhat larger. The biggest difference, however, is the very strong resonance scattering in the majority band for Tc, which together with the large minority scattering, leads to the large total resisitivity of $7.16\,\mu\Omega\,\mathrm{cm/at.\,\%}$ predicted for Tc impurities.

Concerning the band contributions to the conductivity [Fig. 3(c)] the situation is similar to the $3d$ impurities. Except Ag (and Cd) where the majority band is overestimated because of the nonrelativistic treatment, the contributions of $e_6^\uparrow$ and $e_5^\downarrow$ are well balanced for the whole series, and the contributions of $h_4^\uparrow$ and $e_6^\downarrow$ are increased in comparison to the $3d$ transition-metal impurities.

The calculated values for the other impurities are in good agreement with experiment.

C. *sp* impurities

The total resistivity of the $4sp$ and $5sp$ impurities [see Figs. 2(a) and 3(a) and Table IV] show a quadratic de-

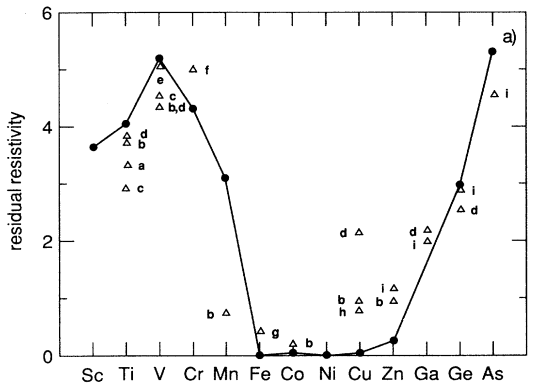

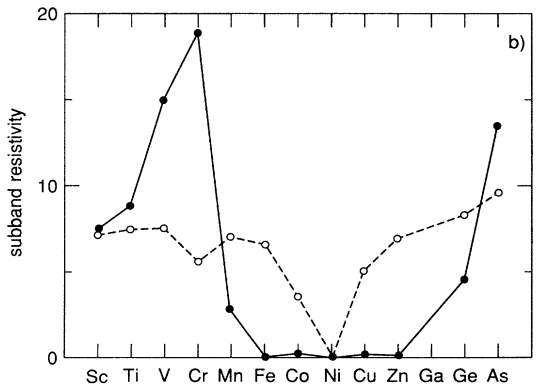

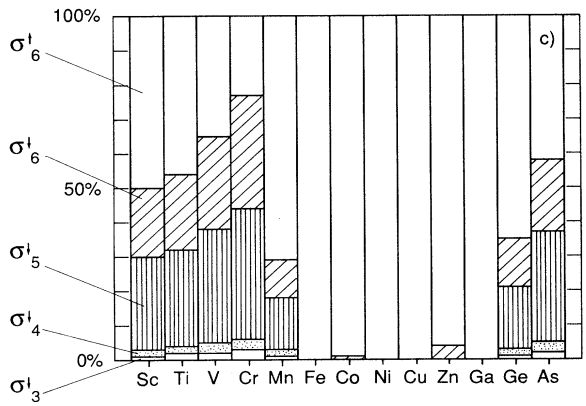

FIG. 2. (a) Calculated residual resistivities for $3d$ and $4sp$ impurities in Ni in comparison to experimental data in $\mu\Omega$ cm/at. %. *a*, see Ref. 3. *b*, see Ref. 7. *c*, see Ref. 8. *d*, see Ref. 36. *e*, see Ref. 37. *f*, see Ref. 4. *g*, see Ref. 2. *h*, see Ref. 38. *i*, see Ref. 33. *j*, see Ref. 35. *k*, see Ref. 39. *l*, see Ref. 34. *m*, see Ref. 5. (b) Subband resistivities $\rho^{\uparrow}$ (full line) and $\rho^{\downarrow}$ (broken line) in $\mu\Omega$ cm/at. %. (c) Relative contributions of the different sheets of the Fermi surface to the conductivity in percent.

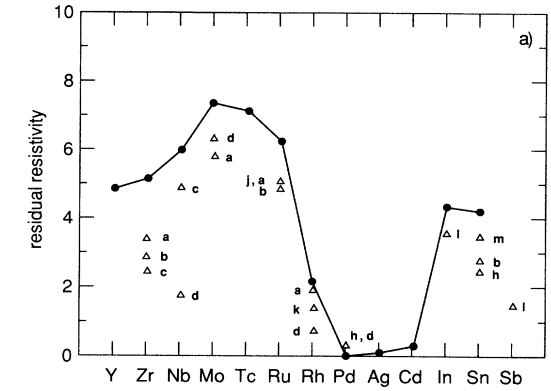

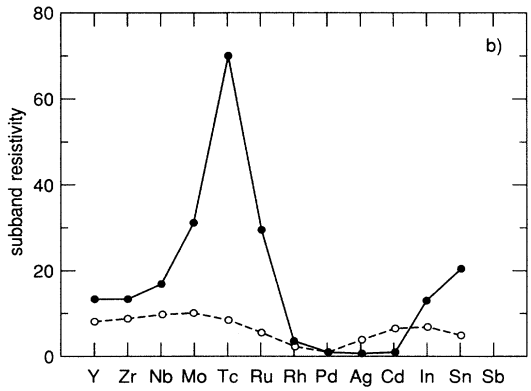

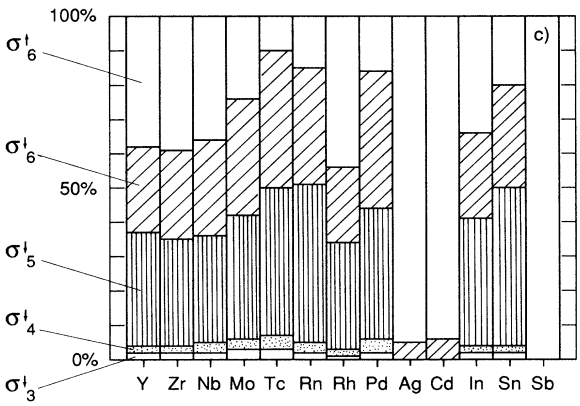

FIG. 3. (a) Calculated residual resistivities for $4d$ and $5sp$ impurities in Ni in comparison to experimental data in $\mu\Omega$ cm/at. %. *a*, see Ref. 3. *b*, see Ref. 7. *c*, see Ref. 8. *d*, see Ref. 36. *e*, see Ref. 37. *f*, see Ref. 4. *g*, see Ref. 2. *h*, see Ref. 38. *i*, see Ref. 33. *j*, see Ref. 35. *k*, see Ref. 39. *l*, see Ref. 34. *m*, see Ref. 5. (b) Subband resistivities $\rho^{\uparrow}$ (full line) and $\rho^{\downarrow}$ (broken line) in $\mu\Omega$ cm/at. %. (c) Relative contributions of the different sheets of the Fermi surface to the conductivity in percent.

TABLE II. Residual resistivities ρ for $3d$ transition-metal impurities in Ni in $\mu\Omega$cm/at.%. Given also are the spin-up and spin-down resistivities, once by including the potential perturbations of the neighboring atoms (ρ, ρ^σ) and once by including only the impurity potential (single-site perturbation: $\rho_{ss}, \rho^\sigma_{ss}$).

ρ	3.67	4.08	5.23	4.35	3.13	0.0000	0.040
$\rho^\uparrow$	7.45	8.86	15.05	18.98	2.91	0.0000	0.041
$\rho^\downarrow$	7.25	7.57	8.02	5.65	7.05	6.50	3.79
ρ_{ss}	3.71	3.77	4.09	3.55	1.84	0.012	0.011
$\rho^\uparrow_{ss}$	8.41	9.77	14.92	18.74	2.50	0.012	0.011
$\rho^\downarrow_{ss}$	6.65	6.14	5.63	4.38	7.03	6.46	3.90

pendence on the valence difference ΔZ, which is known as Linde's rule for *sp* impurities in the noble metals. From the decomposition into spin-up and spin-down contributions as shown in Figs. 2(b) and 3(b) it is obvious that this arises from the relatively weak scattering in the majority band. In the minority band the scattering is much stronger and, quite analogous to the situation for the early *sp* impurities, is essentially determined by missing d states at E_F, which are absent at the impurity site. Therefore the minority band is essentially blocked, and the current is mainly carried by the majority band. The observation of Linde's rule is therefore a direct consequence of the noble metal-like Fermi surface of the majority band and the similar behavior of the spin-up LDOS at E_F for the *sp* impurities in Ni.

By comparing the total resistivities of Table IV as calculated in the single-site approximation with the more accurate values for the perturbed cluster, we see that the single-site values for Zn, Ge, and Cd are larger than the cluster values. This is a paradoxical result, since naively one would expect that the inclusion of additional scattering centers, i.e., the perturbed nearest-neighbor potentials, should increase the resistivity. This idea, however, basically means that the scattering strength of the different scattering centers should add incoherently, which is not the case. Rather, the interference between the scattering at different sites is important, and this can be constructive as well as destructive. Thus it is the destructive interference between the scattering at the impurity and the perturbed nearest-neighbor potentials which leads to a reduced resistivity.

D. Subband ratios $\alpha = \rho^\downarrow/\rho^\uparrow$

Valuable information about the ratio $\alpha = \rho^\downarrow/\rho^\uparrow$ of the subband resistivities can be obtained from resistivity measurements in ternary ferromagnetic alloys.[10] Within the two-band model one obtains for the deviations of the alloy resistivity from Matthiessen's rule

$$\Delta\rho = \rho_{AB} - (\rho_A + \rho_B) = \frac{(\alpha_A - \alpha_B)^2 \rho_A \rho_B}{(1+\alpha_A)^2 \alpha_B \rho_A + (1+\alpha_B)^2 \alpha_A \rho_B}, \quad (15)$$

where A and B indicate the two kinds of impurities and $\rho_A, \rho_B, \rho_{AB}$ the total resistivities of the A and B alloys and the ternary AB alloy. Moreover, α_A and α_B are the corresponding subband ratios, i.e., $\alpha_A = \rho^\downarrow_A/\rho^\uparrow_A, \alpha_B = \rho^\downarrow_B/\rho^\uparrow_B$.

In deriving Eq. (15) one assumes that Matthiessen's rule is well satisfied for the subband resistivities, so that $\rho^\sigma_{AB} = \rho^\sigma_A + \rho^\sigma_B$. This is indeed a good approximation, as we will show in a forthcoming publication. Equation (15) remains invariant, if we simultaneously replace α_A and α_B by their reciprocal values $1/\alpha_A$ and $1/\alpha_B$. This is due to the fact that from a macroscopic measurement like the resistivity it is impossible to say which subband carries most of the current, whether the spin-up subband ($\alpha > 1$) or the spin-down subband ($\alpha < 1$). However, if the ratio α_B is known for a reference B alloy, then the resistivity measurements for the ternary AB alloys allow according to Eq. (15) a unique determination of the ration α_A for the A alloy and especially a decision

TABLE III. Residual resistivities ρ for $4d$ transition-metal impurities in Ni in $\mu\Omega$cm/at.%. Given also are the spin-up and spin-down resistivities $\rho^\uparrow$ and $\rho^\downarrow$, once by including the potential perturbations of the neighboring atoms (ρ, ρ^σ) and once by including only the impurity potential (single-site perturbation: $\rho_{ss}, \rho^\sigma_{ss}$).

	Ni(Y)	Ni(Zr)	Ni(Nb)	Ni(Mo)	Ni(Tc)	Ni(Ru)	Ni(Rh)	Ni(Pd)
ρ	4.87	5.14	6.05	7.37	7.16	6.27	2.23	0.03
$\rho^\uparrow$	12.91	13.15	17.10	30.56	69.30	29.19	3.10	0.19
$\rho^\downarrow$	7.81	8.45	9.36	9.71	7.99	5.02	2.39	0.036
ρ_{ss}	4.49	4.16	4.21	4.51	4.67	4.01	2.41	0.045
$\rho^\uparrow_{ss}$	15.30	14.50	17.60	29.20	61.80	28.40	4.05	0.43
$\rho^\downarrow_{ss}$	6.35	5.85	5.53	5.34	5.05	4.67	2.63	0.051

TABLE IV. Residual resistivities ρ for $4sp$ and $5sp$ transition-metal impurities in Ni in $\mu\Omega$ cm/at. %. Given also are the spin-up and spin-down resistivities $\rho^{\uparrow}$ and $\rho^{\downarrow}$, once by including the potential perturbations of the neighboring atoms (ρ, ρ^{o}) and once by including only the impurity potential (single-site perturbation: ρ_{ss}, ρ_{ss}^{o}).

	Ni(Cu)	Ni(Zn)	Ni(Ge)	Ni(As)	Ni(Ag)	Ni(Cd)	Ni(In)	Ni(Sn)
ρ	0.021	0.28	2.99	5.37	0.17	0.39	4.41	4.27
$\rho^{\uparrow}$	0.021	0.28	4.63	13.53	0.18	0.43	13.01	21.96
$\rho^{\downarrow}$	5.22	6.79	8.41	9.66	4.35	6.56	6.67	5.30
ρ_{ss}	0.021	0.92	3.25	4.69	0.17	0.50	4.52	4.33
$\rho_{ss}^{\uparrow}$	0.022	1.06	6.90	17.30	0.18	0.55	14.30	23.90
$\rho_{ss}^{\downarrow}$	6.03	6.96	6.16	6.44	4.60	6.22	6.61	5.29

whether $\alpha_A > 1$ (transport mostly in the majority band) or $\alpha_A < 1$ (transport mostly in minority band).

Our calculated ratios α are listed in Table V together with the experimentally determined ratios. Note that in most cases we obtain in agreement with the experiment $\alpha < 1$, i.e., the minority band carries most of the current. The extremely large values obtained for Fe, Co as well as Cu, Zn, and Ag, Cd reflect the correct tendency, but should not be taken too seriously, since they are expected to be strongly reduced by spin-orbit coupling. For comparison with the experiments we list in Table V in addition to the calculated value α_{theor} also the reciprocal value $1/\alpha_{\text{theor}}$. The only differences we obtain are for Zr, In, and Sn; there our calculated values are smaller than 1. The experiments deliver $\alpha > 1$.

VI. SUMMARY

The investigation of the residual resistivity in dilute Ni alloys by an *ab initio* calculation shows clearly that the current is carried mostly by the electrons of the majority band, which consist of an admixture of *sp* and *d* states.

TABLE V. Values of $\alpha = \rho^{\downarrow}/\rho^{\uparrow}$ for dilute impurities in Ni.

Impurity	α_{theor}	$(1/\alpha_{\text{theor}})$	α_{expt}
Sc	0.97		
Ti	0.85		0.9,[a] 4,[b] 2.7[d]
V	0.53		0.45,[a] 0.55,[b] 2.3[d]
Cr	0.30		0.21,[a] 0.45,[b] 0.4,[c] 0.21,[d] 0.2,[f] 0.4[g]
Mn	2.42		6.3,[a] 15,[b] 5.4[d]
Fe			11,[a] 20,[b] 7.3[d]
Co	92.4		13,[a] 30,[b] 20,[c] 13,[d] 20,[f] 20[g]
Y	0.60		
Zr	0.64	1.56	7.5[e]
Nb	0.54		0.44,[e] 0.47[i]
Mo	0.31		0.28,[e] 0.37[i]
Tc	0.11		
Ru	0.17		0.075,[a] 0.15[e]
Rh	0.77		0.3,[a] 0.17,[e] 0.29[i]
Pd	0.19		1[d]
Cu	250		2.9,[a] 3.7[d]
Zn	24.0		2.2[a]
Ga			1.7[g]
Ge	1.82		1[g]
As	0.71		
Ag	24		
Cd	15.2		
In	0.51	1.96	1.5[h]
Sn	0.24		1.6,[a] 1.35[h]
Sb			0.8[h]

[a]See Ref. 7.
[b]See Ref. 8.
[c]See Ref. 30.
[d]See Ref. 31.
[e]See Ref. 3.
[f]See Ref. 32.
[g]See Ref. 33.
[h]See Ref. 34.
[i]See Ref. 35.

From the minority electrons only the $e_5^{\downarrow}$ band contributes noticeably.

The two-current model without spin-flip scattering works well for all systems with a residual resistivity larger than 1 $\mu\Omega$ cm at. %. For Fe, Co, Cu, and Ag, Cd impurities in Ni, we obtain too small resistivities since the majority band is essentially unperturbed. Here spin-flip scattering being not included in our calculation has to be taken into account.

The general trend along the transition-metal series is determined by the positions of the virtual bound states. For the *sp* impurities we find a behavior as in the noble metals (Linde's rule), since the current is determined by the majority electrons. In total a consistent picture of the transport properties of Ni alloys is obtained.

ACKNOWLEDGMENTS

One of us (I.M.) wishes to thank the KFA Jülich for financial support and for kind hospitality during several stays at the Institut für Festkörperforschung.

[1]N.C. Mott, Adv. Phys. **13**, 325 (1964).
[2]T. Farrell and D. Greig, J. Phys. C **1**, 1359 (1968).
[3]J. Durand and F. Gautier, J. Phys. Chem. Solids **31**, 2773 (1970).
[4]F.C. Schwerer and J.W. Conroy, J. Phys. F **1**, 877 (1971).
[5]D.C. Price and G. Williams, J. Phys. F **3**, 810 (1973).
[6]D. Greig and J.A. Rowlands, J. Phys. F **4**, 232 (1974).
[7]J.F. Dorleijn and A.R. Miedema, J. Phys. F **5**, 487 (1975).
[8]A. Fert and I.A. Campbell, J. Phys. F **6**, 849 (1976).
[9]J. Yamashita and H. Hayakawa, Prog. Theor. Phys. **56**, 361 (1976).
[10]I.A. Campbell and A. Fert, in *Ferromagnetic Materials*, edited by E. P. Wohlfarth (North-Holland, New York, 1982).
[11]S. Blügel, H. Akai, R. Zeller, and P.H. Dederichs, Phys. Rev. B **35**, 3271 (1987).
[12]N. Stefanou, A. Oswald, R. Zeller, and P.H. Dederichs, Phys. Rev. B **35**, 6911 (1987).
[13]R. Zeller, J. Phys. F **17**, 2123 (1987).
[14]P.T. Coleridge, J. Phys. F **2**, 1016 (1972).
[15]J. van Ek and A. Lodder, Solid State Commun. **73**, 373 (1990).
[16]N.A.M. Holzwarth and M.J.G. Lodder, J. Phys. Condens. Matter **19**, 1961 (1975).
[17]P.M. Oppeneer and A. Lodder, J. Phys. F **17**, 1885 (1987).
[18]P.M. Oppeneer and A. Lodder, J. Phys. F **17**, 1901 (1987).
[19]I. Mertig, E. Mrosan, and P. Ziesche, *Multiple Scattering Theory of Point Defects in Metals: Electronic Properties* (Teubner-Verlag, Leipzig, 1987).
[20]A. Fert, J. Phys. C **2**, 1784 (1969).
[21]A. Bourquart, E. Daniel, and A. Fert, Phys. Lett. **26A**, 260 (1968).
[22]P. Monod, Ph.D. thesis, Université Paris-Sud, 1968.
[23]O. Jaoul and I.A. Campbell, J. Phys. F **5**, L69 (1975).
[24]I. Mertig, E. Mrosan, and R. Schöpke, J. Phys. F **12**, 1689 (1982).
[25]V.L. Moruzzi, J. Janak, and A.R. Williams, *Calculated Electronic Properties of Metals* (Pergamon, New York, 1978).
[26]G. Lehmann and M. Taut, Phys. Status Solidi B **54**, 469 (1972).
[27]P.C. Hohenberg and W. Kohn, Phys. Rev. **136**, B864 (1964).
[28]W. Kohn and L.J. Sham, Phys. Rev. **140**, A1133 (1965).
[29]U. von Barth and L. Hedin, J. Phys. C **5**, 1629 (1972).
[30]P. Leonard, M.C. Cadeville, and J. Durand, J. Phys. Chem. Solids **30**, 2169 (1969).
[31]T. Farrell and D. Greig, J. Phys. C **2**, 1465 (1969).
[32]M.C. Cadeville, F. Gautier, C. Robert, and J. Roussel, Solid State Commun. **7**, 1701 (1968).
[33]J. Hugel, J. Phys. F **3**, 1723 (1973).
[34]R.N. Ross, D.C. Price, and Gwyn Williams, J. Magn. Magn. Mater. **10**, 59 (1979).
[35]J. Durand, Ph.D. thesis, Université Louis Pasteur, 1973.
[36]V.M. Beylin, T.I. Zeynalov, I.L. Rogelberg, and V.A. Cherenkov, Fiz. Met. Metalloved. **46**, 1083 (1978).
[37]S. Arajs, H. Chessin, and R.V. Colvin, Phys. Status Solidi B **7**, 1009 (1964).
[38]D. Greig and J.A. Rowlands (unpublished).
[39]M.C. Cadeville and J. Durand, Solid State Commun. **6**, 399 (1968).
[40]H. Ehrenreich, H.R. Philipp, and D.J. Olechna, Phys. Rev. **131**, 2469 (1963).